Opto-Electronics Review

Method to determine solar-blind ultraviolet energy and electrical corona loss relation

Casper J. Coetzer[a]*, Hermanus C. Myburgh[a], Nicolas West[b], Jerry Walker[c]

[a] Department of Electrical, Electronic and Computer Engineering, University of Pretoria, Hatfield 0028, South Africa
[b] Department of Electrical and Information Engineering, University of Witwatersrand, Johannesburg, Wits 2050, South Africa
[c] Walmet Consultancy (Pty) Ltd, Powerville, Vereeniging 1939, South Africa

Article Info	Abstract
	Solar-blind ultraviolet cameras as part of high-voltage electrical inspections until recently have mostly been used for pure observations. These observations only imply the presence of corona discharges and not the severity thereof. A radiometric algorithm together with a calibration algorithm to perform an optical energy measurement were presented earlier. This is a guide on how to apply the algorithm to determine the total optical measurement from corona discharges, plus additional processing. This guide and additions are used to compare the electrical and optical domains with actual examples. The main objective is to illustrate how to determine the electrical and optical relation for the IEC 60720 high-voltage electrical test configurations using a standard open procedure.

1. Introduction

The combination of solar-blind ultraviolet (SBUV) and visual images by SBUV cameras used for high-voltage inspection is shown in Fig. 1 [1, 2]. The SBUV type cameras use a special image intensifier and a solar-blind filter technology that enable the corona detection[1–4].

Figure 2 shows some of the challenges associated with the current optical energy processing techniques to analyse the SBUV images using pixel counting. This is based on the number of active pixels using various methods as discussed previously [4, 5]. Figure 2 consists of two images of a point-to-plane electrical test. At a setting of 16 kV$_{RMS}$, the SBUV counts are approximately 83 counts, and at 29 kV$_{RMS}$, the camera indicates 116 counts for the same camera settings. The corresponding electrical loss of the same experiment is reported by Fig. 3 which is 48 pC (picocoulombs) for 16 kV$_{RMS}$ and approximately 2400 pC for 29 kV$_{RMS}$. The objective of this paper is to illustrate how the electrical energy loss of Fig. 3. and the optical SBUV flux relation can be determined using the open radiometric optical measurement methodology [6, 7].
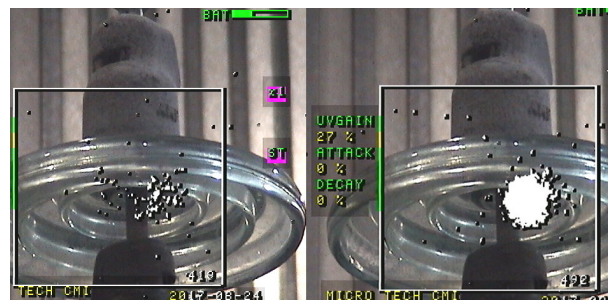

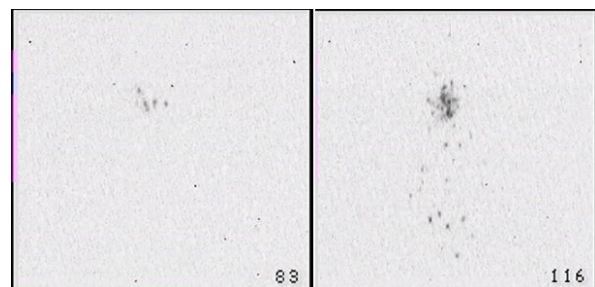**Fig. 1.** Electrical corona discharges as observed by combined visual and SBUV images of an insulator.

Fig. 2. Inverted SBUV image of corona of a point-to-plane test at 16 kV$_{RMS}$ giving 83 counts and 29 kV$_{RMS}$ resulting in 116 counts.

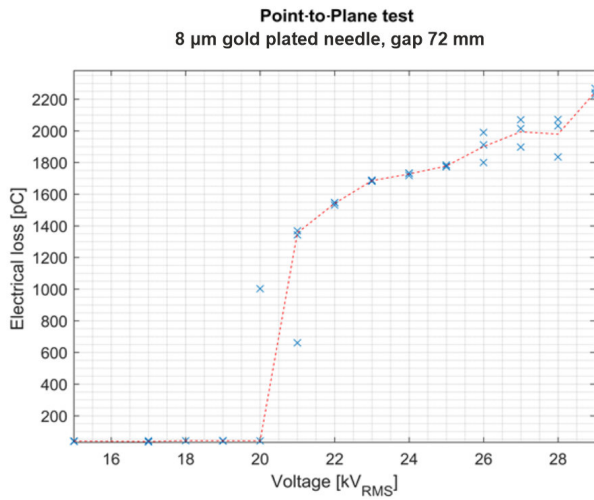*Corresponding author at: casper.coetzer.uv@gmail.com

Fig. 3. Electrical loss of a glass insulator at the WITS University High Voltage Laboratory.

2. Current measurements methodologies

2.1. Sensitivity and counts

The SBUV camera specifications currently contain only one optical radiometric unit referred to as the 'sensitivity' with typical values of 2.05×10^{-18} with units [W·cm^{-2}] [8]. This is actually the lowest detectable optical flux by an SBUV camera [9].

Optical flux is currently measured by a non-standard unit known as counts per second. The counts units are based on the typical measurement associated with the image intensifier and the CMOS detector topology [3, 10, 11].

There are shortcomings with the count method which can be summarized as follows [4]:

- Count is a non-standardized measurement unit.
- Results are dependent on observation distance.
- It is influenced by camera focus setting.
- Cannot deal with measurement fluctuations.

2.2. Indicative results for electrical investigations

Although the count method is a non-radiometric optical measurement method, it only provides indicative results of the optical flux and electrical losses in the case of electrical corona discharge observations.

One such an investigation is by Chunyan *et al.* who used a standard SBUV camera and its counts to investigate electrical point-to-plane alternating current (AC) test configurations [12]. The results implied that the electrical loss and optical SBUV have the same response for electrical discharge and optical flux (unit of [W]) *vs.* voltage. However, measurements differed from each other for different gap sizes, different distances, and different camera gain settings. Furthermore, they noted measurements variations at different focus settings.

Zhuansun, in another investigation, found a parabolic relation between corona current and optical count for the point-to-plane test configuration direct current (DC) case, also investigated the electrical loss *vs.* SBUV observations [13].

Another approach that provided good indicative electrical *vs.* camera results is a number of studies that used the adaptive neuro-fuzzy inference with an adaptive network-based fuzzy inference system (ANFIS) [14]. Notable is the work of Wang *et al.* who used the ANFIS algorithm to create an estimation function of the electrical *vs.* optical signal in counts [15].

The only report to date that claims this is a standard radiometric measurement is Maistry *et al.* using an electronic shutter, but there are many questions on some of the details of the algorithm [16]. One question is whether the use of a shutter might have an effect on the optical measurement as it is not synchronized with the electrical discharges.

Although all these results provide a good estimation of the electrical corona loss and the optical flux relation with the counting output, the experiments are not comparable (non-standardised). This difference is best highlighted by Li *et al.* using two cameras from different manufacturers [17]. They concluded that there was a constant 1.3-fold difference between two different cameras counting results.

This has led to the creation of an alternate open standardized radiometric algorithm [5]. It is shown in the subsequent sections how this open algorithm is applied to electrical discharge and optical SBUV investigations.

3. Standardized measurement method

3.1. Step 1: Radiometer

Figure 4 shows additional steps to consider as part of the electrical *vs.* optical investigations. It shows that the first step is to use a radiometer or a reference camera (golden reference) to calibrate the reference source for subsequent steps as part of the process [18]. Secondly, measurements at a reference source are translated to a local source setup at the r_s distance These translated measurements are then used to adjust the (local) source to known source values for calibrating SBUV cameras.
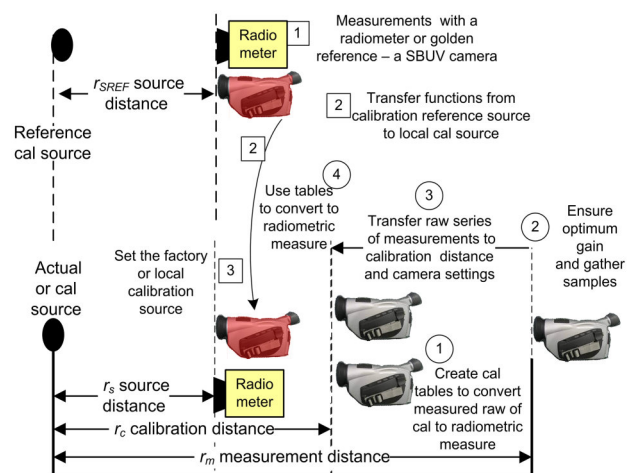

Fig. 4. Outline of the calibration and measurement methodology.

3.2. Step2: Rudimentary measurements

Based on the algorithm, a rudimentary optical measurement model of the SBUV camera is illustrated in Fig. 5. The optical source is presented by the area A_0, the
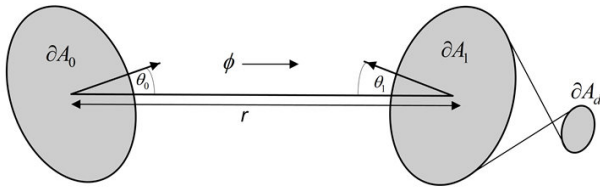
Fig. 5. Rudimentary source and camera model.

SBUV camera input aperture A_1, and the entire detector area A_d. The figure shows the optical flux ϕ (unit of watts [W] in radiometry) from the source to the camera and the distance r between the camera and the source [3, 19].

Instead of using active (on/off) pixel counting, it is

$$d_{SUM} = \sum_{i=1}^{x_i \times y_i} d_i \quad \text{for} \quad d_i > T_{BCK} \qquad (1)$$

with the unit digital level [DL] which is the summation of the pixel digital values d_i that are more than the background signal threshold T_{BCKG} [5]. A more enhanced version of (1) that can deal with Raleigh scattering is

$$d_{SUM} = \sum_{\text{Cluster } i=1}^{\text{Cluster } x_i \times y_i} d_i \quad \text{for} \quad d_i > T_{BCK} \qquad (2)$$

which sums pixels identified in hotspot cluster areas. Hotspots are identified with a spatial filter that was explained as part of the alternative SBUV detector proposed and presented by this team previously [20, 21].

3.3. Step 3: Multiple samples to deal with variations

Figure 6 shows the results of (1) for consecutive images. It highlights that the optical values using (1) fluctuate when observing the SBUV flux from a glass insulator. The time interval between each image in the series is derived from the camera frame rate per second of 20 ms or 40 ms depending on the camera frame rate. The average (X_{MEAN}) of Fig. 6 of 100 frames (N) is 3.59×10^5 and is determined by the relationship

$$X_{MEAN} = \frac{\sum_{n=1}^{N} d_{SUM}(n)}{N-1} \qquad (3)$$

Fortunately, it can be concluded here that the values in this example only fluctuate by about 9.4% according to the calculated coefficient of variation (CV) [22]. This implies that the SBUV camera observations can be regarded as stable enough for measurements. That is if the camera settings results in a stable measurement. To attain optimum stable camera measurements, parameters such as the CV and the number of saturated pixels are used as part of the algorithm [5]. However, occasionally, the camera measurement algorithm must eliminate measurements in the time-series measurements that deviate too much from the majority of measurements [5]. These variations are the result of the Cherenkov radiation (appears as sporadic blobs) and occasional electrical discharges [3, 5]. The camera processing time here is 2 s as this is how long it
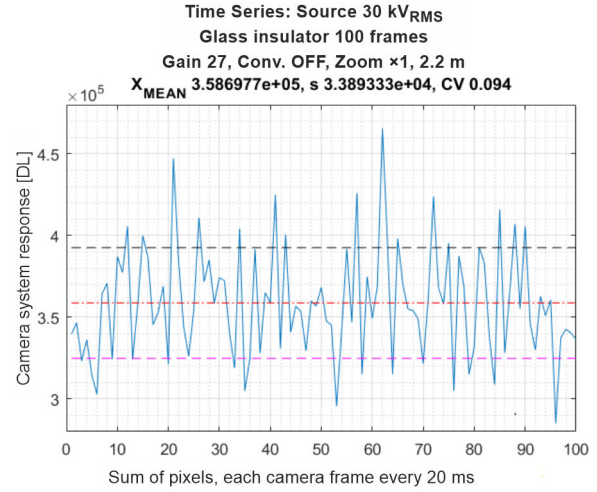

Fig. 6. Processing of 100 consecutive frames with pixel summation.

takes to collect 100 samples at a 20 ms frame rate. This can be shortened with fewer samples.

This averaged (X_{MEAN}) value from multiple samples is used throughout for all raw and calibrated measurements.

3.4. Step 4: Using camera calibration tables

The raw X_{MEAN} camera measurement using (1) [and (3)] is transferred to the optical International System of Units (SI) using a number of calibration transfer functions [5]. To obtain these transfer functions, a calibration procedure is used together with a reference source that provides a set of transfer functions which is briefly summarised below.

3.4.1. Dynamic transfer function

Using an adjustable SBUV source (Fig. 4) with a known output flux, the dynamic transfer function of an SBUV camera can be described by

$$d_E = a_m E + c_m , \qquad (4)$$

where d_E is the digital summation output of the camera using (1) [or (2)], a_m is the gradient coefficient, E is the source irradiance at a particular distance, and c_m is the offset. To create a transfer function for multiple samples per calibration source, the flux value (4) is expanded to

$$X_{MEAN}(f(E)) = a_m E + c_m \qquad (5)$$

implying that the dynamic transfer function is created from a series of measurements at each source flux level [18]. Both (4) and (5) are straight line estimations for narrowband calibration sources. Personal experience with wideband sources has resulted in camera responses that are third-order polynomials. In this introductory guideline, a narrowband source with a straight-line approximation is used to convey introductory aspects, suggesting that the more elaborated case of a wideband source and the full camera spectral response will be presented later.

3.4.2. Gain transfer function

A dynamic relation such as (4) is obtained at a particular camera gain and a zoom setting which implies that multiple

dynamic transfer functions need to be created during calibration [5]. The use of these multiple dynamic graphs implies that the gain transfer function must be known to translate the measurement from one gain to another. The X_{MEAS} measurement with the g_{MEAS} camera gain setting can be transferred onto a calibration curve (5) for the g_{TARGET} gain to the point with the value of $X_{GTARGET}$ with

$$X_{GTARGET} = \left(e^{b_g g_{TARGET}} \cdot e^{-b_g g_{MEAS}}[X_{MEAS} - c_g]\right) + c_g \quad (6)$$

with the gain coefficient b_g measured at a particular fixed distance and c_g – the camera measurement offset.

3.4.3.   Distance transfer function

As with gain transfer (6), X_{MEAS} measurements performed at the r_{MEAS} distance need to be transferred to another $X_{RTARGET}$ value at the r_{TARGET} distance that has a calibration curve. The distance translation to use is

$$X_{RTARGET} = (r_{MEAS}^2 \cdot r_{TARGET}^{-2}[X_{MEANZ} - c_{MEAS}]) + c_{MEAS} , (7)$$

where c_{MEAS} is the camera offset. This transfer function was derived from the distance translation function

$$X_R = X_{ORIGIN} \frac{a_r e^{b_r r}}{r^2} + c_r \quad (8)$$

with the X_{ORIGIN} measurement at distance 0, c_r – the measurement offset, a_r – the constant, b_r – the total atmospheric attenuation, and the X_R measurement at the r distance.

3.4.4.   Zoom transfer functions

The particular SBUV camera (Corocam 504) used in the experiments demonstrated that it has the ability to observe sources with two different zoom settings of 1 and 0.5. It was shown previously how to transfer measurements from one zoom setting to another zoom setting [5]. The two zoom relationships are

$$X_{MEANz05} = \left(m_{z05} m_{z1}^{-1}[X_{MEANMEASz1} - c_{z1}]\right) + c_{z05} \quad (9)$$

and

$$X_{MEANz1} = \left(m_{z1} m_{z05}^{-1}[X_{MEANMEASz05} - c_{z05}]\right) + c_{z1} \quad (10)$$

where $X_{MEANz05}$ is the zoom times 0.5 that is transferred from the measured $X_{MEANMEASz1}$ (zoom 1), X_{MEANz1} for the zoom times 1 is transferred from the measured $X_{MEANMEASz05}$ for a zoom times 0.5, c_{z05} is the offset for the zoom times 0.5, c_{z1} is the offset for the zoom times 1, m_{z05} is the gradient of output function for the zoom times 0.5, and m_{z1} is the gradient of output for the zoom times 1.

3.5.   Derivation and additional details

There are additional parameters such as the lens map and the spectral response that can be included for optical measurements to improve accuracy, but here the focus is to provide an outline of the electrical loss *vs.* the optical SBUV measurement procedure [18, 19].

4.   Electrical *vs.* optical

4.1.   Electrical setup

Figure 7 illustrates the first type of electrical test setup to use for electrical an optical experiments in accordance with IEC 60720 standards [23]. It illustrates that the point-to-plane test subject is connected in parallel with a measurement circuit which contains the coupling capacitor C_k and a narrowband filter with a preamplifier. The measurement signals illustrated here are as follows:

1. A high voltage supply signal with discharge pulses as a result of corona discharges.
2. An attenuated high voltage signal measurable with an oscilloscope between C_k and the preamplifier.
3. The low frequency power cycle is removed by filtering leaving only pulses.
4. The electrical pulses are integrated and averaged resulting in an energy measurement referred to as a partial discharge measurement here using a specialized instrument, the ICMcompact [4].
5. An SBUV camera is used for optical measurements. The optical result was expected to be similar to the electrical result, as indicated in Fig. 7.
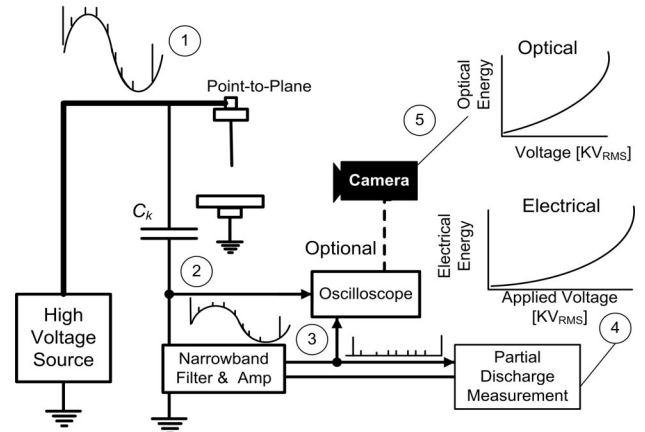

Fig. 7. Parallel electrical test configuration circuit diagram for a point-to-plane showing typical electrical and optical results.

4.2.   Electrical measurements

Figure 8 is a typical oscilloscope measurement at the preamplifier input on channel 1 of the oscilloscope (no. 2 of Fig. 7), including the preamplifier output (no. 3 of Fig. 7) on channel 2. Channel 1 is the attenuated power cycles (here 50 Hz) and the corona discharge pulses.

Corona discharge pulses are used for electrical loss measurements. They are an indirect measurement of the charge transfer q of the current pulse $i(t)$ described by

$$q = \int i(t) = (C_a + C_b)\delta V_a \quad (11)$$

with δV_a – the voltage over the test subject plus void (gap), C_a – the capacitance thereof, C_b – the capacitance of the test subject [24]. Using the gap voltage δV_c is

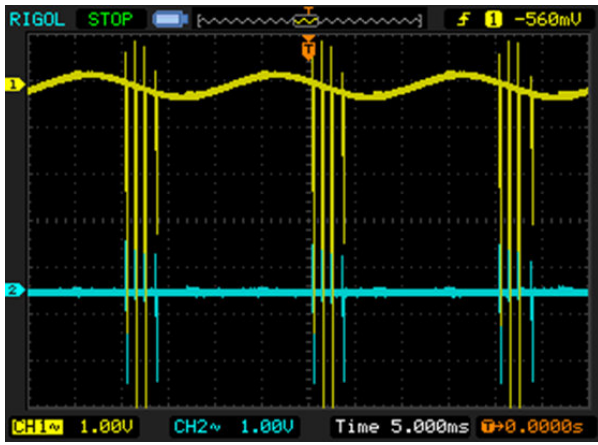$$\delta V_c = C_b^{-1}(C_a + C_b)\delta V_a \quad (12)$$

Fig. 8. Point-to-plane measurement with an oscilloscope prior to the electrical preamplifier (top) and after the preamplifier (bottom).

which means that (11) can be rewritten in the indirect measure form as

$$q_{app} = C_b \delta V_b , \qquad (13)$$

the apparent charge. The discharge electrical power P [W] is a summation of q_{app} pulses over the T time with

$$P = T^{-1} \sum_{i=1}^{\text{in time } T} q_i u_i \qquad (14)$$

with u_i being the instantaneous values of the test voltage.

Figure 9 depicts consecutive partial discharge measurements of q_{app}, each point presenting a series of pulses by the ICMcompact in [pC] [24]. An analysis of the electric time series values shows a variation of 2.3% (CV = 0.023), implying a set of stable measurements [22].
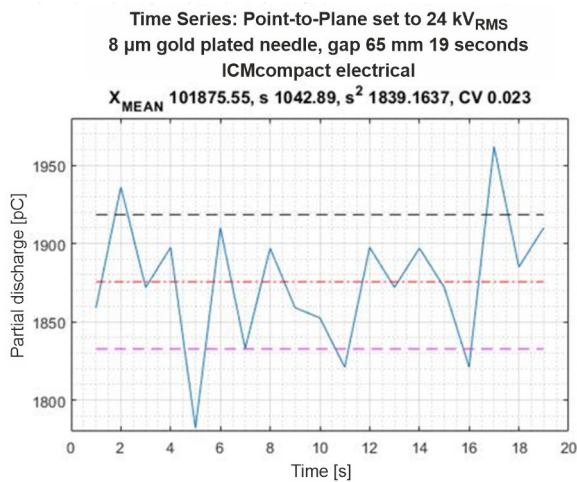

Fig. 9. Time series of electrical discharge samples at a particular voltage collected by a partial discharge instrument (ICMcompact).

5. Point-to-plane electrical experiment

The first electrical test evaluation using the electrical configuration of Fig. 7 is a point-to-plane electrical test as observed in Fig. 10. The figure shows the combined visual and SBUV image and the SBUV-only image.
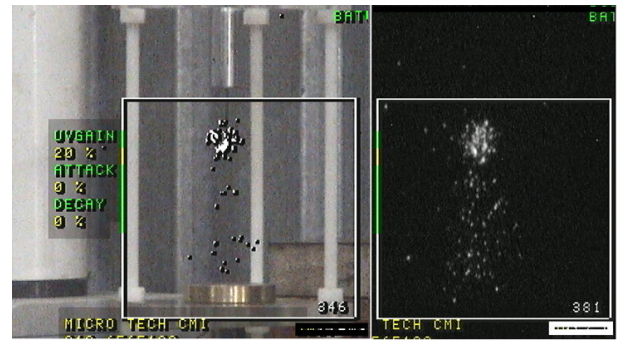

Fig. 10. Point-to-plane images. Visual and solar-blind ultraviolet images combined (left). Solar-blind ultraviolet image only (right).

5.1. Electrical measurement

Figure 3 showed the electrical loss of the point-to-plane test in [pC] *vs*. voltage applied.

Each point in the graph consists of several samples (similar to Fig. 9) collected at a particular voltage setting.

5.2. Optical measurement

Figure 11 depicts the SBUV camera raw [DL] measurements for the point-to-plane which electrical loss was reported in Fig. 3. Each point of the graph here consists of 150 frames (samples), each created with (3). Figure 11 also shows the response of the camera when no signal is present with horizontal lines. These three 'Bck' lines are derived from the no-signal distributions of the camera using (3). Actual signal (blue and red) and the blank signal distributions (black) are later compared in Fig. 12 and Fig. 13. Note also the signal and blank distributions shown as part of Fig. 11. The horizontal lines indicate the no-signal average (Bck Avg), the upper 95% confidence line (Bck Top), and the lower 95% confidence line (Bck Bot).
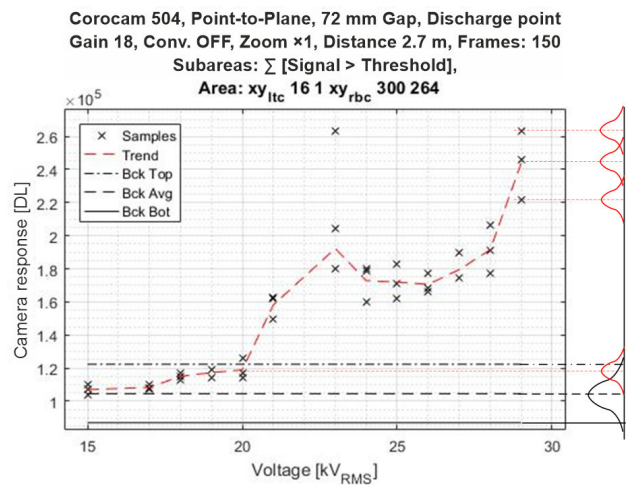

Fig. 11. SBUV for a 72 mm point-to-plane gap and voltage applied. (Gauss distributions are provided for points).

Figure 12 provides a comparison of the SBUV camera samples for a 20 kV$_{RMS}$ and background (no-signal) distribution fitted to a Gauss distribution [22]. Each distribution is derived from 150 frames each point attained by (1). Figure 12 also shows that that the sample average is to the left of the right-hand limit line of the blank signal
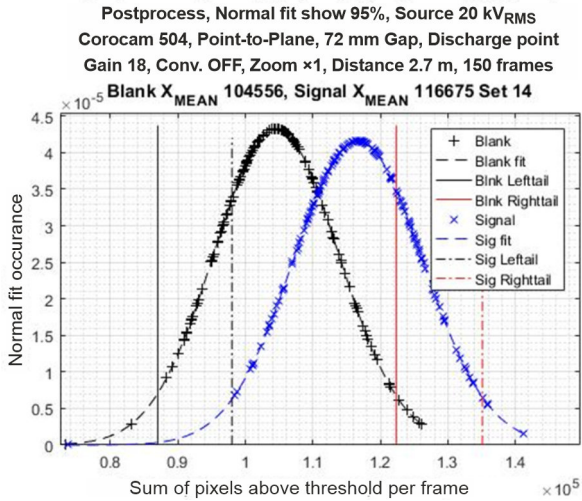
Fig. 12. Distribution of solar-blind ultraviolet measurements for a 72 mm point-to-plane gap and 20 kV$_{RMS}$ voltage applied *vs*. no signal.

('Blank Righttail'), which implies that the 20 kV$_{RMS}$ result is too low to be regarded as a valid measurement. Figure 13, on the other hand, shows that the average of the camera samples for 29 kV$_{RMS}$ is far to the right of the Blank Righttail, suggesting the measurement at this voltage is distinguishable from a no-signal value.
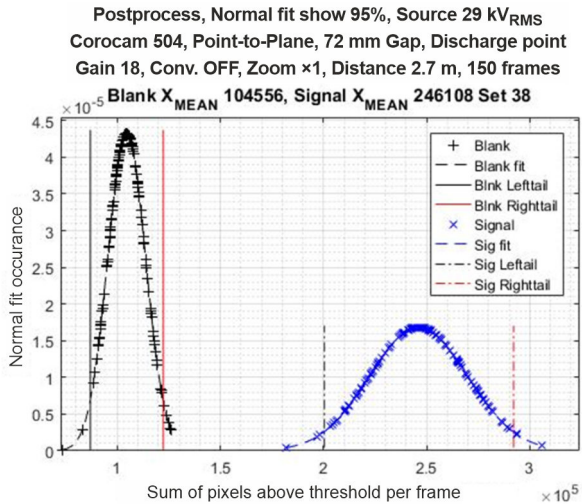

Fig. 13. Distribution of SBUV measurements for a 72 mm point-to-plane gap and 29 kV$_{RMS}$ voltage *vs*. no signal.

Each optical SBUV camera observation with (1) and (3) at a set voltage (such as Fig. 13) is collected and translated (converted) to irradiance [W·m^{-2}] by an open algorithm resulting in Fig. 14 [5].

5.3. Optical and electrical relation

After measuring the electrical energy (Fig. 13) and the optical SBUV flux (Fig. 14), the objective is to determine the relationship. The electrical loss can be converted from pC to watt using the measurement time. However, the total optical SBUV flux to calculate is usually somewhat challenging as it is the irradiance E which is defined as an optical flux per area [W·m^{-2}] related to a measurement
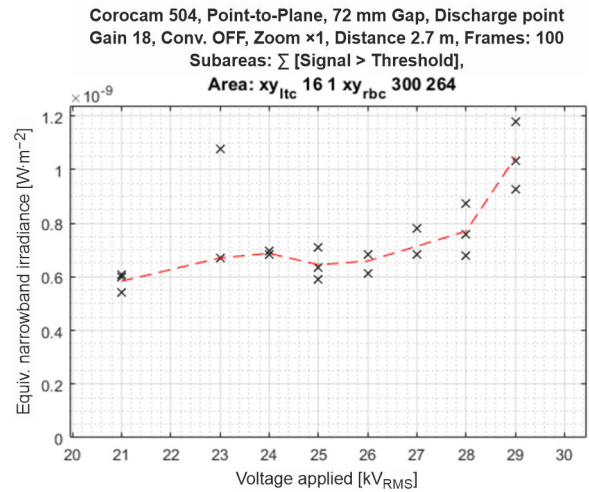

Fig. 14. Solar-blind ultraviolet measurements for a 72 mm point-to-plane gap with voltage applied.

distance [18, 19]. Fortunately, the total optical SBUV flux of a source can be determined by modelling irradiance as a sphere with a low atmospheric attenuation for SBUV at short distances [8]. The total flux is modelled by a narrowband source (from calibration) as an equivalent narrowband optical flux

$$\phi_{NB} = E_{NB}\pi r^2 , \qquad (15)$$

where r is the distance and E_{NB} is the narrowband irradiance of Fig. 14. Each point in Fig. 14 is translated to the optical flux value ϕ_{NB}.

Figure 15 shows the relation between the total optical SBUV and the electrical energy using the values of Fig. 3 and translates the values of Fig. 14 with (15). The resulting relation between optical flux and electrical loss is

$$\phi_{NB} = 3.96 \times 10^{-14}P_{pC}^2 - 1.17 \times 10^{-10}P_{pC} \\ + 1.11 \times 10^{-7} \qquad (16)$$

with ϕ_{NB} – the narrowband equivalent optical flux in units of watts [W] and the electrical loss P_{pC} in units of [pC].
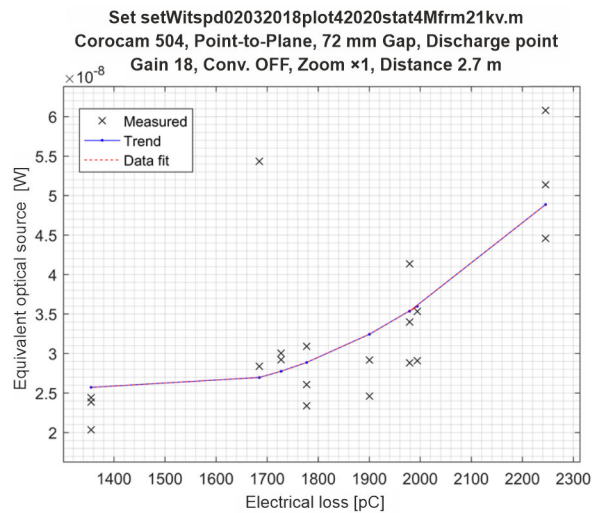

Fig. 15. SBUV measured relation with electrical loss for a 72 mm point-to-plane for 21 kV$_{RMS}$ to 30 kV$_{RMS}$.

5.4. *Different plane gap sizes*

Figure 16 shows the camera measurement result for different point-to-plane gap sizes.
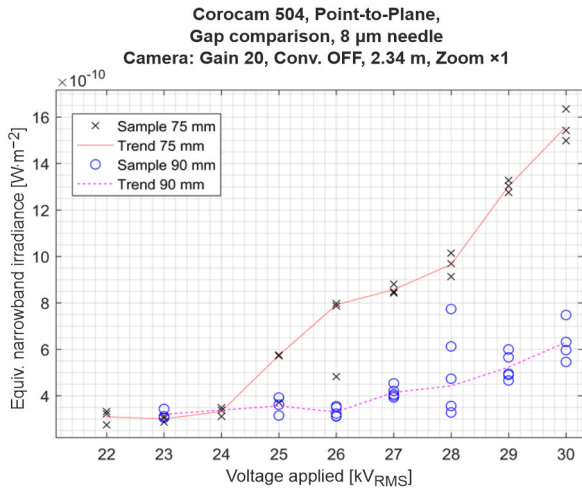

Fig. 16. Optical measurements of different point-to-plane gap sizes *vs.* voltage applied.

These optical results are similar to electrical loss measurements by other researchers, confirming the relationship between the optical and electrical domains [24]. Further analysis in terms of SBUV optical power and electrical loss is left for the future.

6. Glass insulator experiment

The second test set uses a glass insulator (Fig. 1) instead of a point-to-plane using the circuit in Fig. 7 to investigate the electrical loss and optical relation with the open radiometric algorithm.

6.1. *Electrical measurement*

Figure 17 depicts the electrical losses for a glass insulator of Fig. 1. Note that the voltages are higher than in the point-to-plane experiment. They must be used for the glass insulator before the electrical loss and optical SBUV can be detected.
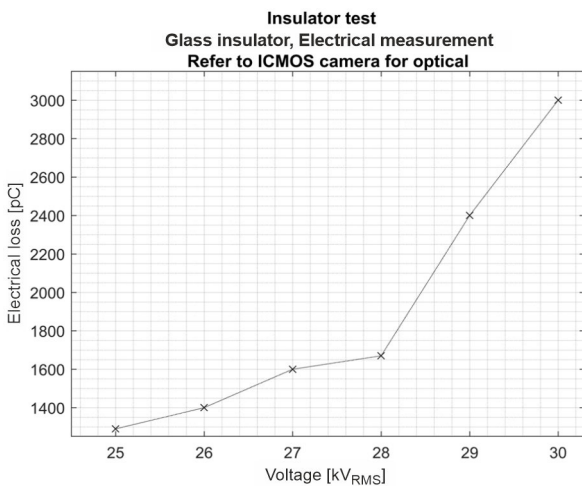

Fig. 17. Electrical corona for a glass insulator.

6.2. *Optical measurement*

Figure 18 reports the camera equivalent narrowband optical SBUV flux of the insulator using the algorithm.
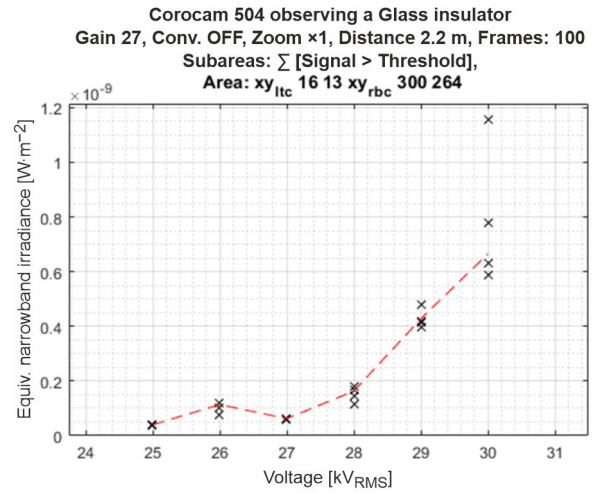

Fig. 18. SBUV optical irradiance for a glass insulator *vs.* voltage.

As with other results, each point on the graph represents 100 samples each at the camera frame rate. More than one set of 100 samples per voltage were made. These multiple sets of results from 25 to 29 kV$_{RMS}$ are similar except at 30 kV$_{RMS}$, which is where the results diverge. An outlier rejection procedure was used to obtain a result from the multiple sets (of 3) per voltage [5].

6.3. *Optical and electrical relation*

The optical SBUV flux and electrical loss relation for the glass insulator is shown in Fig. 19 [9, 22]. Similar to the point-to-plane experiment, the SBUV flux and electrical loss relation is

$$\phi_{NB} = 9.07 \cdot 10^{-16} P_{pC}^2 + 9.139 \cdot 10^{-13} P_{pC} - 2.1 \cdot 10^{-9}. \qquad (17)$$
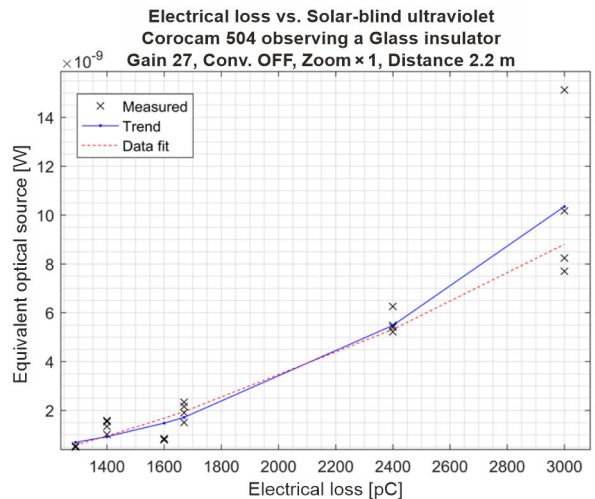

Fig. 19. Electrical corona loss and SBUV optical relation for a glass insulator.

The fitted line visually approximates a straight line as presented in Fig. 19. This implies that different high voltage configurations and parts have different responses. There are additional atmospheric conditions to consider such as air pressure, humidity, and wind that can be taken into account to improve measurements [16, 25, 26].

7. Point-to-plane compared with insulator

Figure 20 provides a comparison of the point-to-plane and the insulator results reported here.
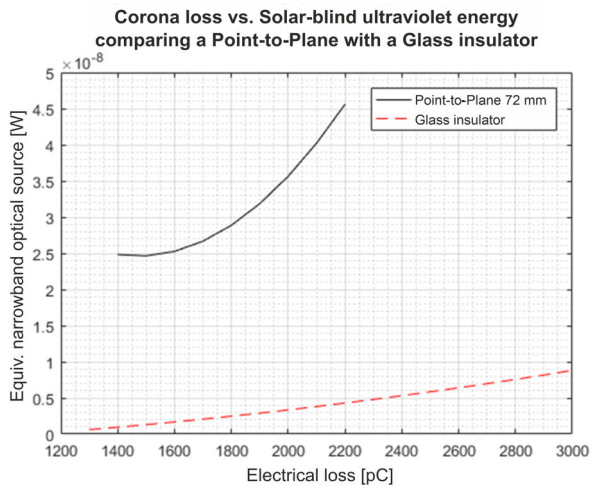

Fig. 20. Comparison of the electrical corona loss and the SBUV optical relation for a point-to-plane test setup and a glass insulator.

8. Conclusions

It was initially noted that the optical flux observed by SBUV cameras in the electrical domain is presented in a non-standard measurement unit of counts. This is highlighted by the measurement differences between SBUV camera manufacturers counting outputs from the same source.

A guide was provided on how to use a standardized optical SBUV measurement for electrical test configurations to find the electrical loss and the standard optical flux relation. Results showed that the optical results differ for the two test configurations.

In addition to the standardized measurement method and unit and guideline, a rudimentary model to measure the total optical SBUV flux was added. The radiometric measurement values were converted (projected) to the optical flux emitted in the source with units [W] for the purpose of comparison with the electrical (15) which also has the unit [W] in future research. This made it possible to determine the electrical loss and observed optical relationships using standardized comparisons and measurements.

Furthermore, the following aspects should also be incorporated in future investigations for purposes of measurement enhancements:

- A wideband calibration source response should be used as opposed to the narrow band source presented here. Although the Planck source is a wideband source that is favoured by some camera manufacturers, it has a

spectral function that is spectrally skew and not similar to actual corona discharges. A solution to overcome this will be presented later.
- Incorporation of the camera spectral response as part of the calibration procedure should also be included.
- Ensuring that all cameras respond in the same manner, especially with regard to the dynamic transfer function, should also be incorporated as part of the calibration and measurement process to be presented later.
- It can be argued that the electrical *vs.* optical results presented here in [pC] should also include u_i from (14). This would allow to compare the optical flux with units [W] with the electrical results of (14) also with units [W].

References

[1] Gubanski, S., Dernfalk, A., Andersson, J. & Hillborg, H. Diagnostic methods for outdoor polymeric insulators. *IEEE Trans. Dielectr. Electr. Insul.* **14**, 1065–1080 (2007). https://doi.org/10.1109/TDEI.2007.4339466

[2] Lindner, M., Elstein, S., Lindner, P., Topaz, J. M. & Phillips, A. J. Daylight Corona Discharge Imager. in *1999 Eleventh International Symposium on High Voltage Engineering* **4**, 340–352 (IEEE, 1999). https://doi.org/10.1049/cp:19990864

[3] Bass, M. *et al. Handbook of optics, Volume II: Design, fabrication and testing, sources and detectors, radiometry and photometry*, (McGraw-Hill, Inc., 2009).

[4] Coetzer, C. *et al.* Status Quo and Aspects to Consider with Ultraviolet Optical versus High Voltage Energy Relation Investigations. in *Fifth Conference on Sensors, MEMS, and Electro-Optic Systems* **11043**, 1104317 (SPIE, 2019). https://doi.org/10.1117/12.2501251

[5] Coetzer, C. J. & West, N. Radiometric calibration and measurement algorithm for electrical inspection solar-blind ultraviolet cameras. *Opto-Electron. Rev.* **30**, e140128 (2022). https://doi.org/10.24425/opelre.2022.140128

[6] Suhling, K., Airey, R. W. & Morgan, B. L. Optimisation of centroiding algorithms for photon event counting imaging. *Nucl. Instrum. Methods Phys. Res. A.* **437**, 393–418 (1999). https://doi.org/10.1016/S0168-9002(99)00770-6

[7] Boksenberg, A., Coleman, C., Fordham, J. & Shortridge, K. Interpolative centroiding in CCD-based image photon counting systems. *Adv. Electron. Electron. Phys.* **64**, 33–47 (1986). https://doi.org/10.1016/S0065-2539(08)61601-7

[8] Coetzer, C.,Vermrulen, H. J. & Herbst, B. M. Aspects that need to be considered for the calibration of ultraviolet solar-blind cameras used for electrical inspection. in *International Conference Insulator News & Market Report (INMR)* 273–301 (2013).

[9] Coetzer, C., Groenewald, S. & Leuschner, W. An analysis of the method for determining the lowest sensitivity of solarblind ultraviolet corona cameras. in *2020 International SAUPEC/Rob-Mech/PRASA Conference* 1–6 (IEEE, 2020). https://doi.org/10.1109/SAUPEC/RobMech/PRASA48453.2020.9040997

[10] Fordham, J., Moorhead, C. & Galbraith, R. Dynamic-range limitations of intensified CCD photon-counting detectors. *Mon. Not. R. Astron. Soc.* **312**, 83–88 (2000). https://doi.org/10.1046/j.1365-8711.2000.03155.x

[11] Bergamini, P. *et al.* Performance evaluation of a photon-counting intensified CCD. in *EUV, X-Ray, and Gamma-Ray Instrumentation for Astronomy VIII* **3114**, 250–259 (SPIE, 1997). https://doi.org/10.1117/12.283773

[12] Chunyan, Z. *et al.* Study on application of ultra-violet instrument in external insulation detection of electric device. in *2008 International Conference on High Voltage Engineering and Application* 391–393 (IEEE, 2008). https://doi.org/10.1109/ICHVE.2008.4773955

[13] Zhuansun, X. *et al.* The impact of negative DC corona discharge on the ultraviolet photon count in rod to plane air gaps. in *2015 IEEE Conference on Electrical Insulation and Dielectric Phenomena (CEIDP)* 362–365 (IEEE, 2015). https://doi.org/10.1109/CEIDP.2015.7352091

[14] Jang, J.-S. R. Fuzzy modeling using generalized neural networks and kalman filter algorithm. in *AAAI* **91**, 762–767 (1991).

[15] Wang, S., Lv, F. & Liu, Y. Estimation of discharge magnitude of composite insulator surface corona discharge based on ultraviolet imaging method. *IEEE Trans. Dielectr. Electr. Insul.* **21**, 1697–1704 (2014). https://doi.org/10.1109/TDEI.2014.004358

[16] Maistry, N., Schutz, R. A. & Cox, E. The quantification of corona discharges on high voltage electrical equipment in the UV spectrum using a corona camera. in *2018 International Conference on Diagnostics in Electrical Engineering (Diagnostika)* 1–4 (IEEE, 2018). https://doi.org/10.1109/DIAGNOSTIKA.2018.8526024

[17] Li, Z. *et al*. Effects of different factors on electrical equipment UV corona discharge detection. *Energies* **9**, 369 (2016). https://doi.org/10.3390/en9050369

[18] Wyatt, C. *Radiometric calibration: theory and methods*. (Elsevier, 2012).

[19] Willers, C. J. *Electro-Optical System Analysis and Design: a Radiometry Perspective*. (SPIE Press, 2013). https://doi.org/10.1117/3.1001964

[20] Coetzer, C., Becker, T., West, N. & Leuschner, W. Investigating an alternate detector for solar-blind ultraviolet cameras for high-voltage inspection. in *2021 Southern African Universities Power Engineering Conference/Robotics and Mechatronics/Pattern Reco-gnition Association of South Africa (SAUPEC/RobMech/PRASA)* 1–6 (IEEE, 2021) . https://doi.org/10.1109/SAUPEC/RobMech/PRASA52254.2021.9377216

[21] Pratt, W. *Digital Image Processing Wiley-Interscience*. (New York, 2007).

[22] Montgomery, D. C. & Runger, G. C. *Applied Statistics and Probability for Engineers*. (John Wiley and Sons, 2014).

[23] Sze, M. & Lahance, M. High Voltage test techniques-partial discharge measurements. in *Guide for Partial Discharge Mesurements on Medium Voltage (MV) and High Voltage Aparatus*. (IEC, 2000).

[24] Kuffel, E. & Zaeungl, W. *High Voltage Engineering Fundamentals* (Pergamon Press, Oxford, 1984).

[25] Da Costa, E. G., Ferreira, T. V., Neri, M. G., Queiroz, I. B. & Germano, A. D. Characterization of polymeric insulators using thermal and UV imaging under laboratory conditions. *IEEE Trans. Dielectr. Electr. Insul.* **16**, 985–992 (2009). https://doi.org/10.1109/TDEI.2009.5211844

[26] Pinnangudi, B., Gorur, R. & Kroese, A. Quantification of corona discharges on nonceramic insulators. *IEEE Trans. Dielect. Electr. Insul.* **12**, 513–523 (2005). https://doi.org/10.1109/TDEI.2005.1453456